Supporting Information

Ultrafine Co_2P Nanorods Wrapped by Graphene Enables Long Cycle Life Performance for Hybrid Potassium-Ion Capacitor

Yixuan Wang,[a] Zhongyu Zhang,[b] Guangxia Wang,[a] Xinyi Yang,*[a] Yongming Sui,[a] Fei Du,*[b] and Bo Zou*[a]

[a] State Key Laboratory of Superhard Materials, College of Physics, Jilin University, Changchun, 130012, People's Republic of China.

[b] A Key Laboratory of Physics and Technology for Advanced Batteries (Ministry of Education), College of Physics, Jilin University, Changchun, 130012, People's Republic of China.

E-mail: yangxinyi@jlu.edu.cn
dufei@jlu.edu.cn
zoubo@jlu.edu.cn

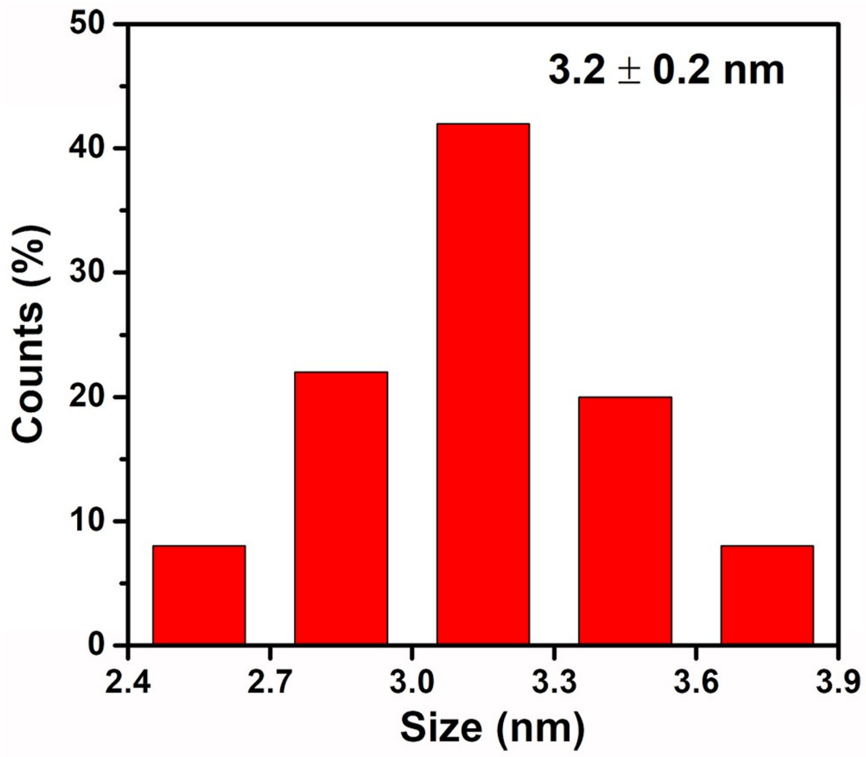

Fig. S1 The diameter distribution of synthesized ultrafine Co_2P NRs.

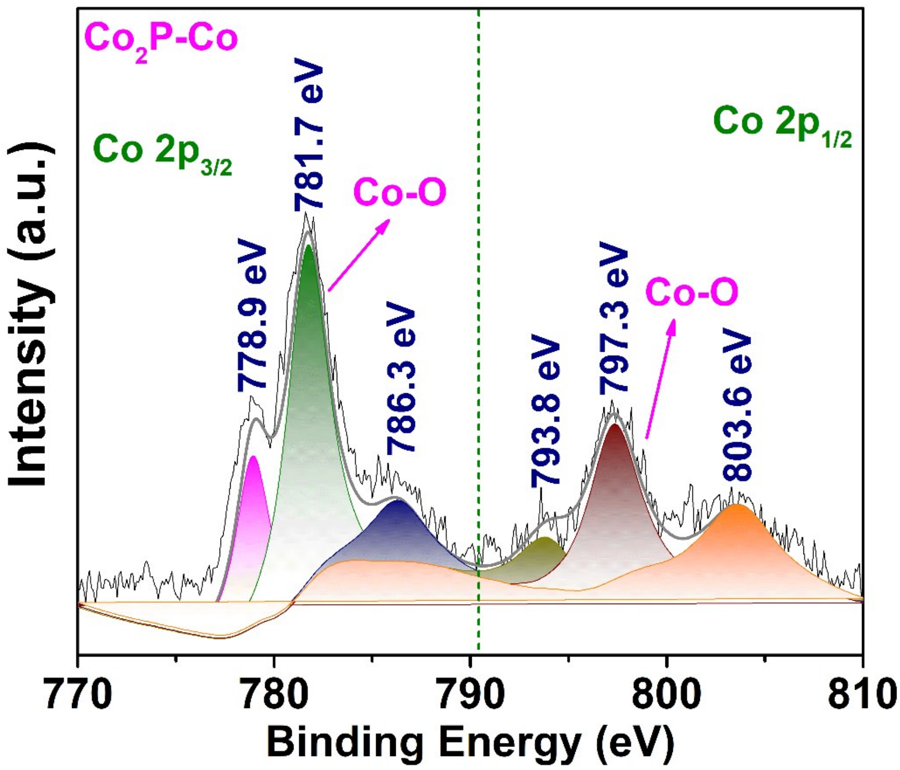

Fig. S2 XPS analysis of pure Co_2P

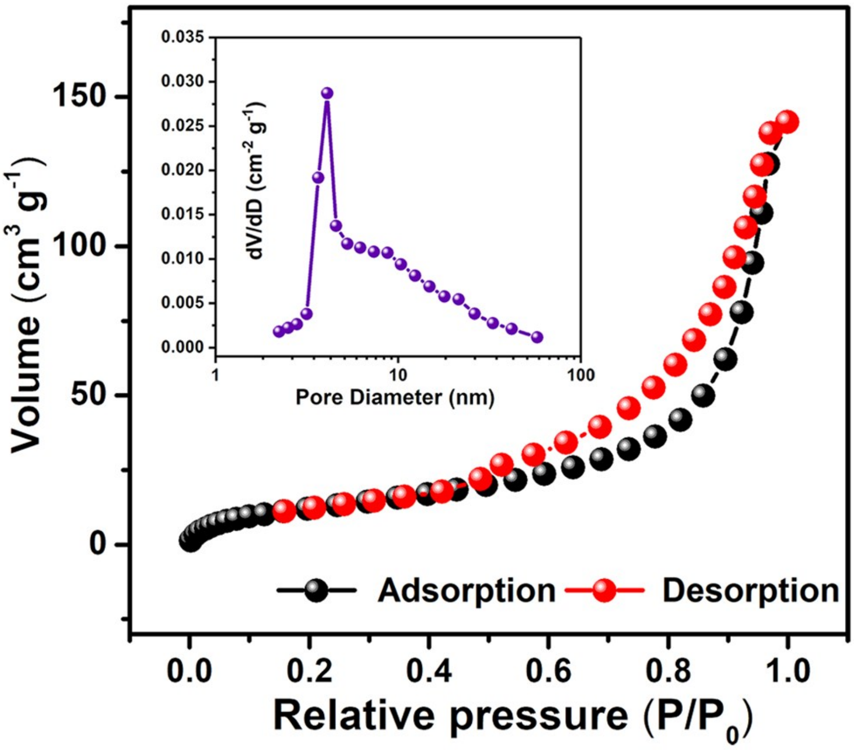

Fig. S3 N_2 adsorption-desorption isotherms and pore-size distribution (inset) of U-Co_2P@rGO-14 nanocomposite.

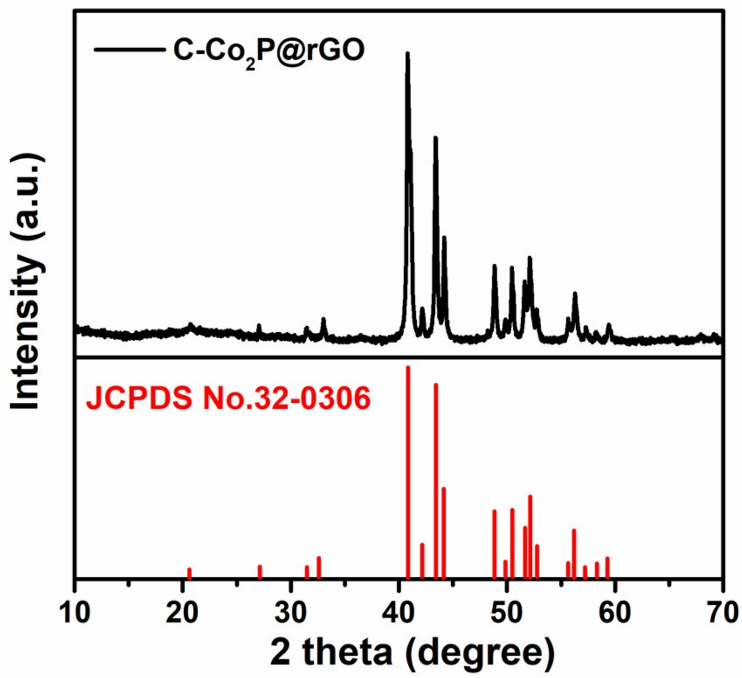

Fig. S4 XRD pattern of the C-Co_2P@rGO powder. All diffraction peaks agree well with an orthorhombic Co_2P phase (JCPDS No. 32-0306) and can be indexed using a unit cell with a = 5.646 Å, b = 6.609 Å, and c= 3.513 Å (space group of *Pnma*).

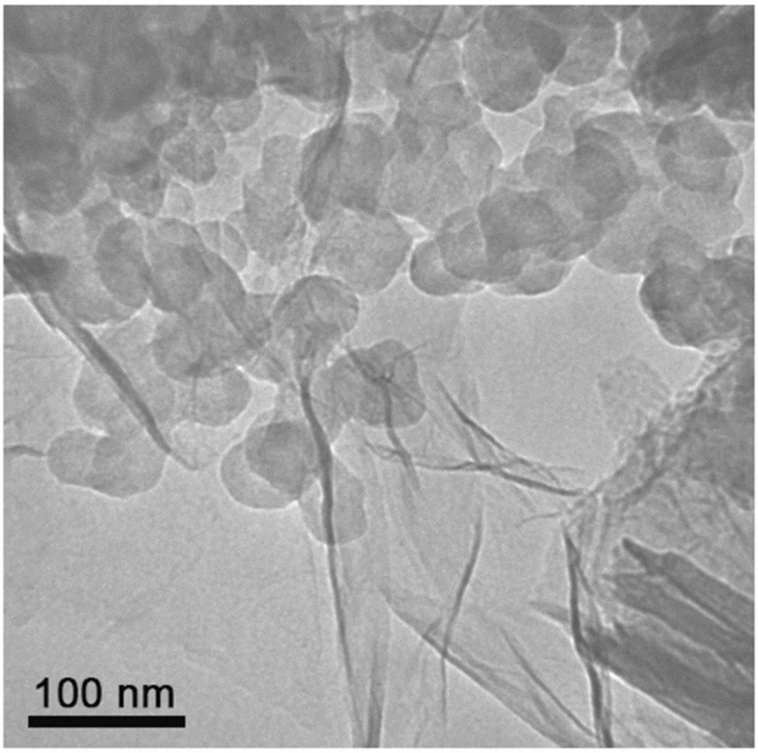

Fig. S5 TEM image of C-Co_2P@rGO. The Co_2P mainly consists of irregular agglomerated micrometer sized particles. The agglomerated microparticles consist of many crystalline nanoparticles around 50 nm, distributed in the amorphous carbon matrix.

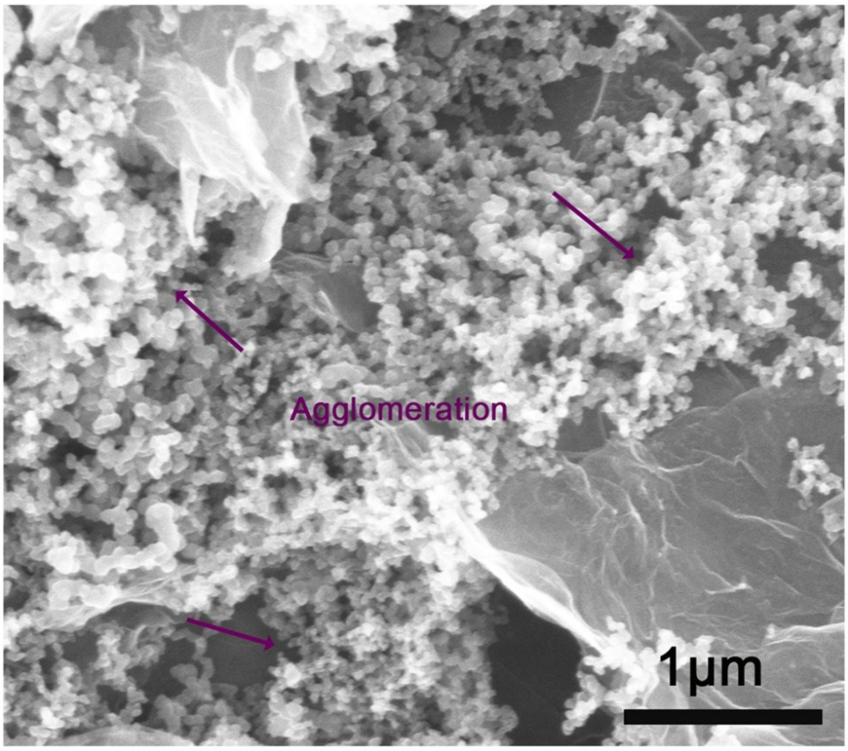

Fig. S6 SEM image of agglomerated C-Co_2P@rGO composite.

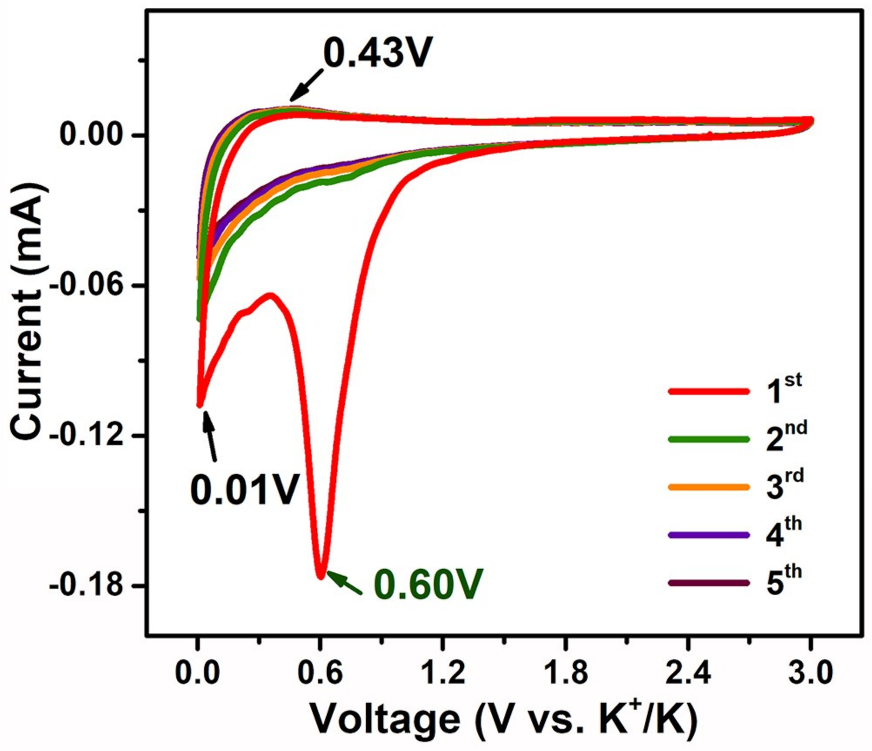

Fig. S7 Cyclic voltammograms for the first five cycles of rGO.

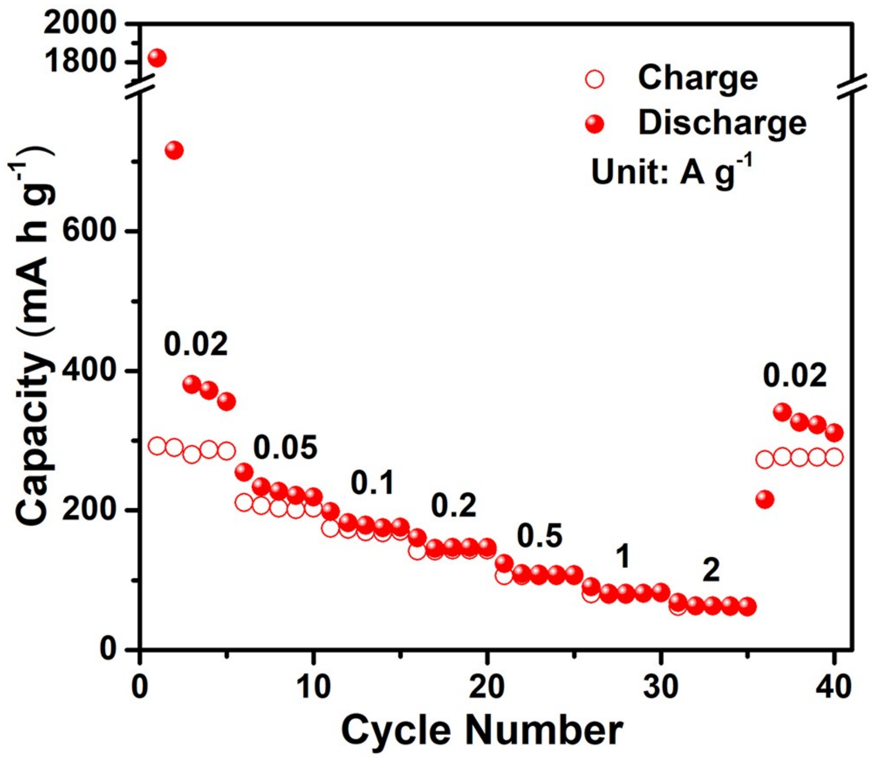

Fig. S8 Rate performance of rGO at different current densities.

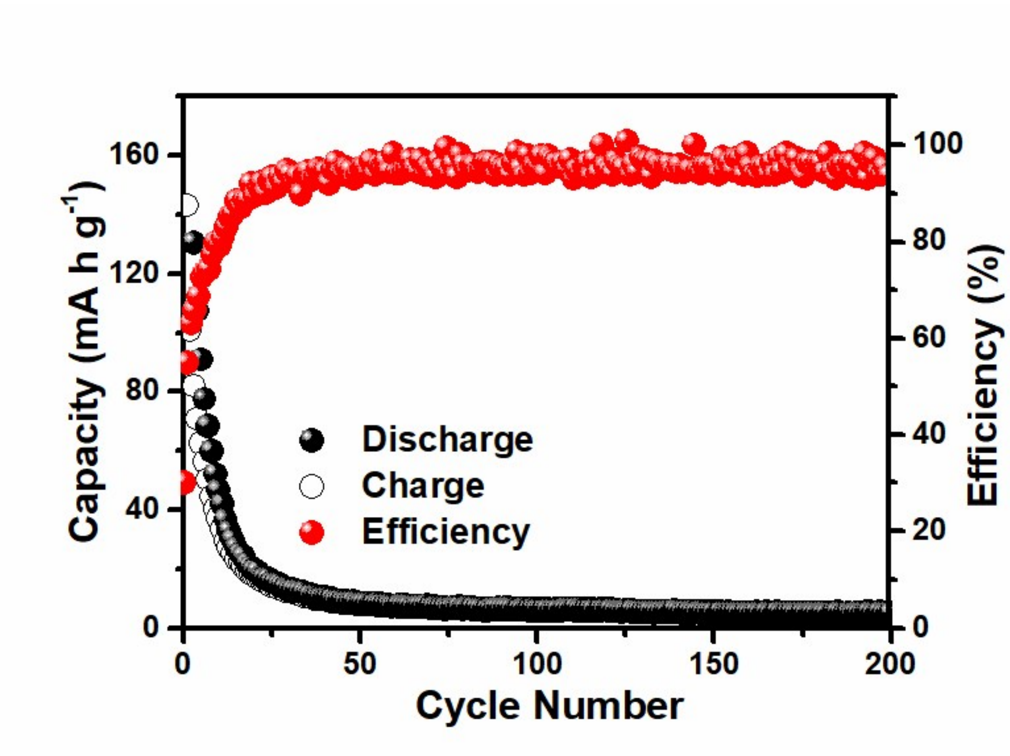

Fig. S9 Long-term cycling of U-Co_2P at a current density of 200 mA g^{-1}.

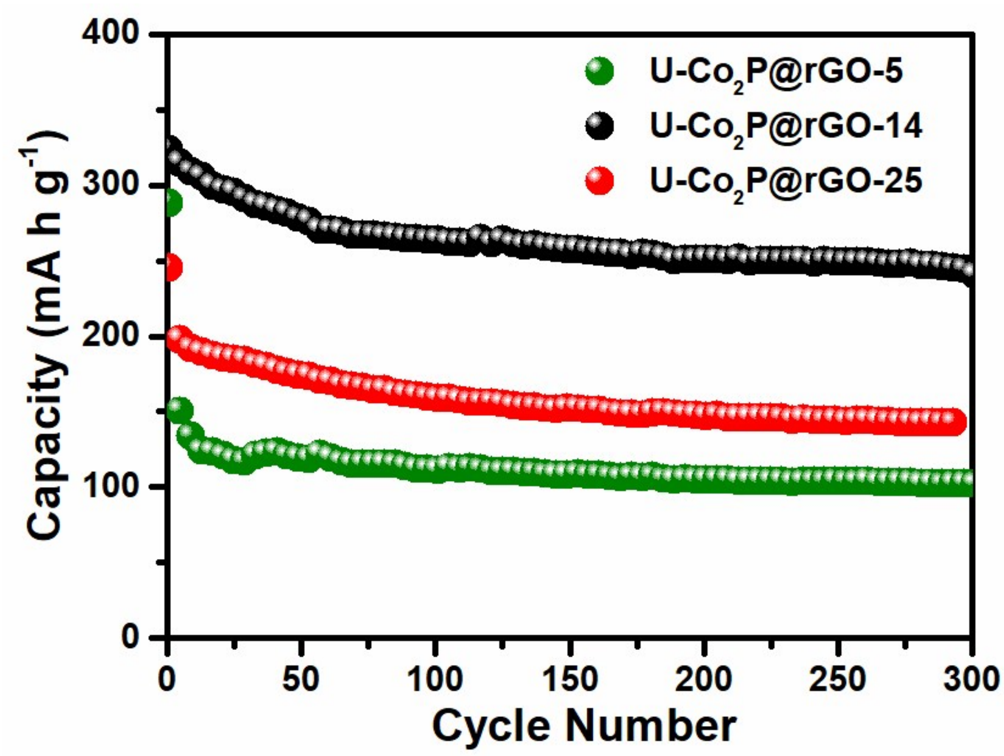

Fig. S10 Cycling performance of U-Co_2P@rGO-5, U-Co_2P@rGO-14 and U-Co_2P@rGO-25 electrodes.

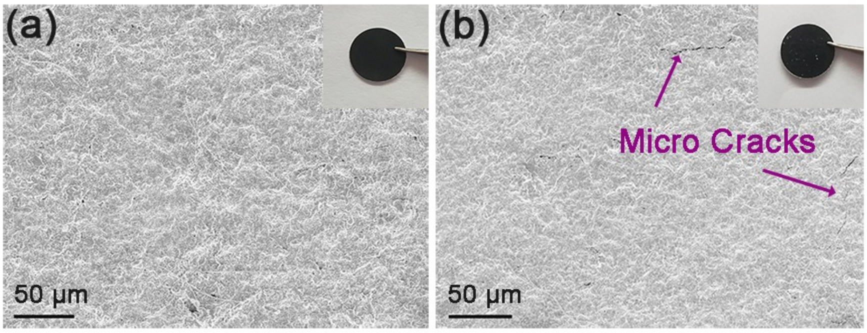

Fig. S11 *Ex-situ* FESEM images for (a) pristine, after (b) the 50th cycle of U-Co_2P@rGO-14 electrodes. Insets show corresponding digital photographs of the electrodes.

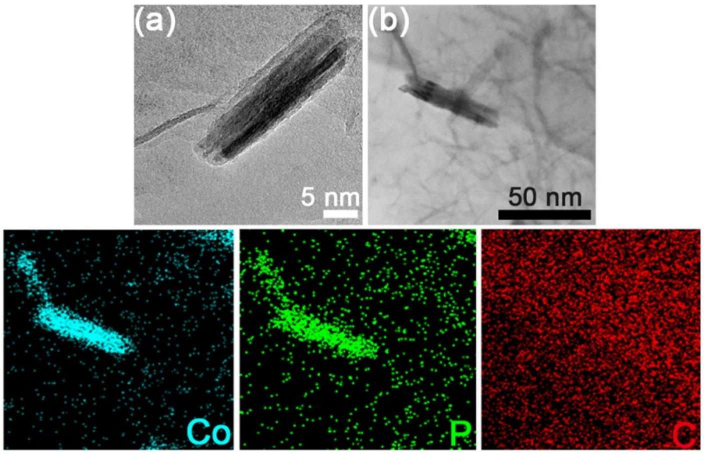

Fig. S12 Long-term cycle performance of U-Co_2P@rGO-14 and structure feature of U-Co_2P@rGO-14 electrodes after the 200th cycle. a) High-magnification TEM, and (b) STEM elemental mapping of U-Co_2P@rGO-14 after the 200th cycle at current density of 200 mA g^{-1}.

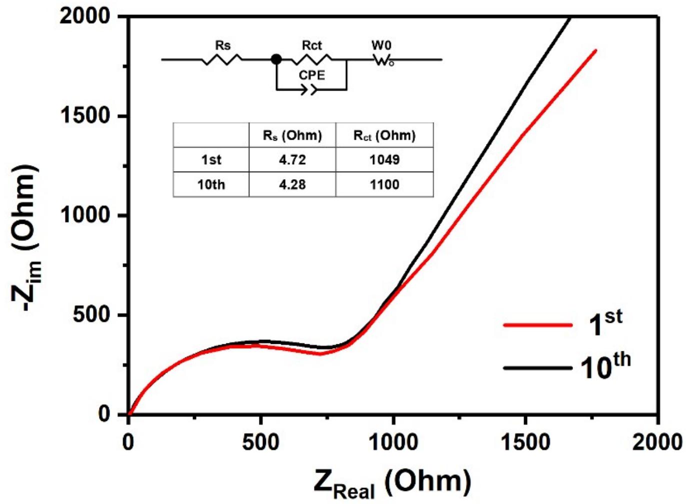

Fig. S13 Electrochemical Impedance Spectroscopy (EIS) of U-Co_2P@rGO-14 after 1st cycle and after 10th cycle.

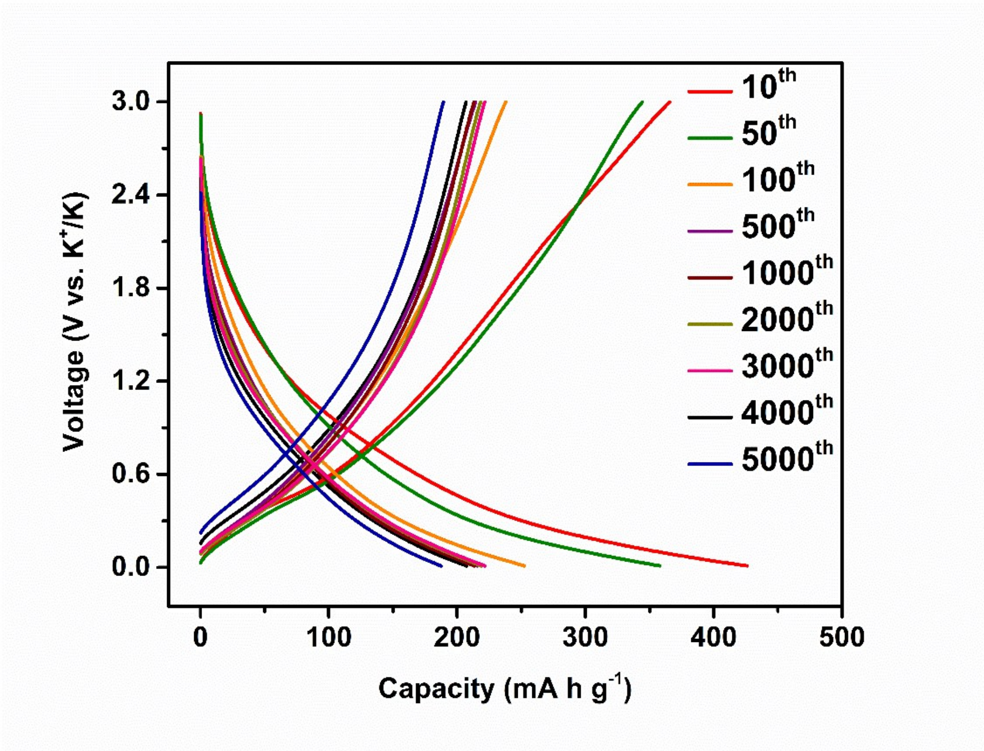

Fig. S14 Galvanostatic charge-discharge curves at a current density of 200 mA g^{-1} in the voltage range of 0.01-3.0 V from 10th cycle to 5000th cycle.

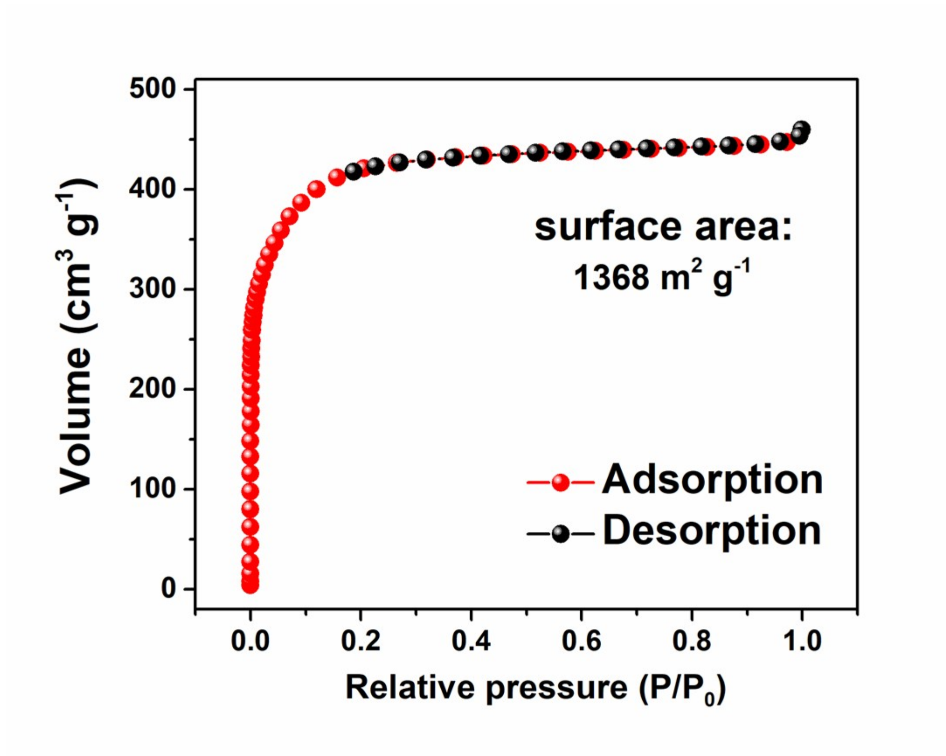

Fig. S15 N_2 adsorption-desorption isotherm of AC.

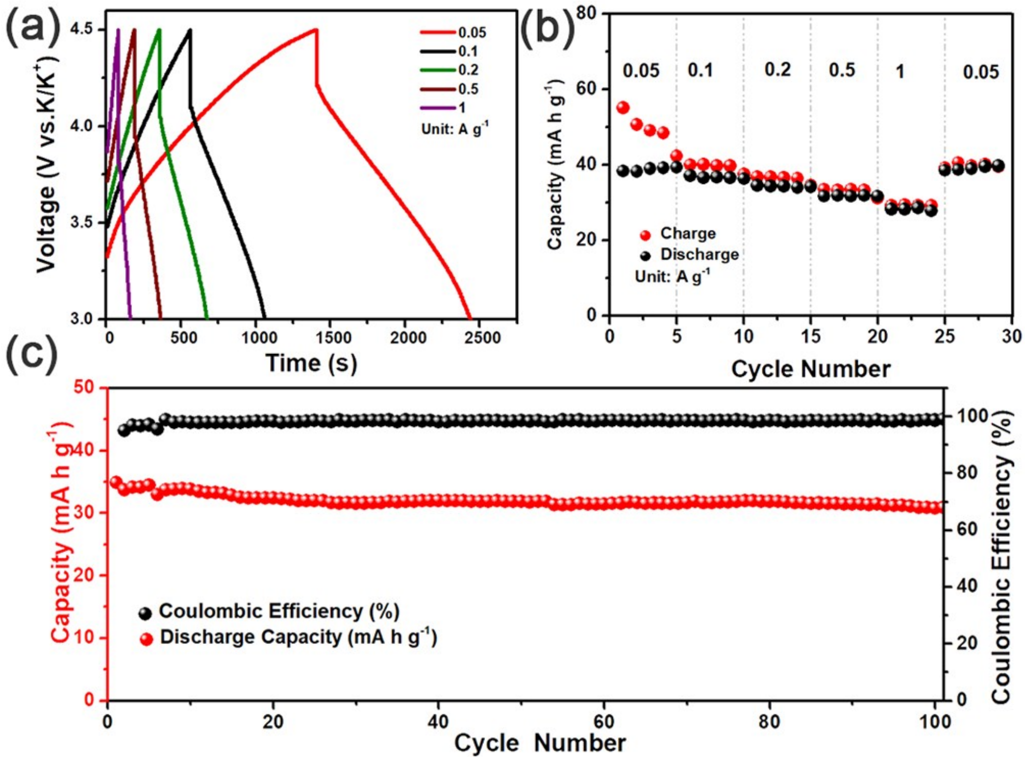

Fig. S16 (a) Galvanostatic discharge-charge curves at different current densities. (b) Rate performance of AC at different current densities and (c) Long-term cycle performance of AC at current density of 0.2 A g^{-1} for 100 cycles in half cell.

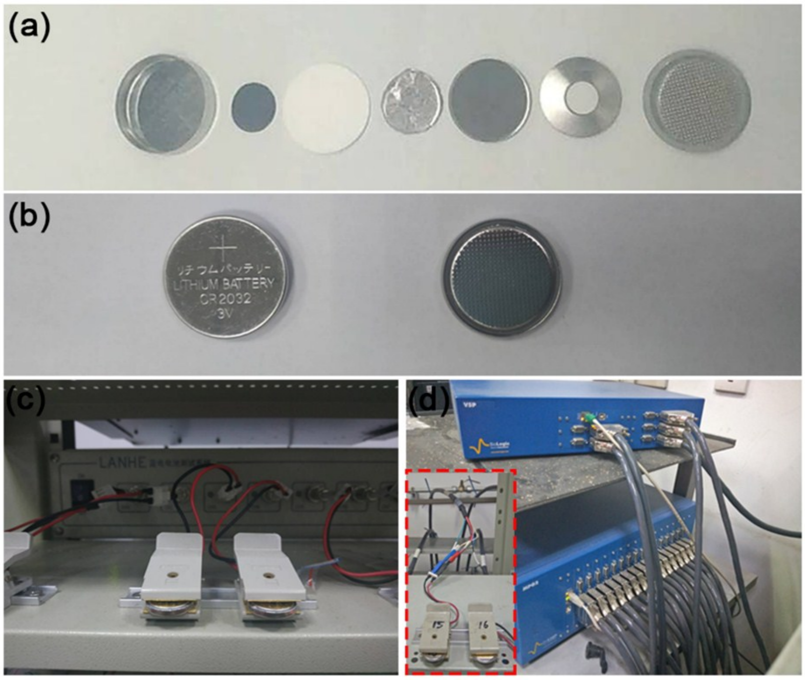

Fig. S17 The photograph of the electrochemical setup and the measurement system, (a) the composition of the coin cell, (b) the assembled coin cell, (c) the Land-2001A (Wuhan, China) automatic battery tester. (d) the VSP multichannel potentiostatic-galvanostatic system.

The electrochemical setup we used is the common coin cell. As shown in Fig. S17a, the composition of the coin cell we used, which includes electrode shell of working electrode, working electrode, separator, potassium, current collector, leaf spring and electrode shell of counter electrode are exhibited in order, based on the assembled step. After a step-by-step assembled process, the coin cell is presented in Fig. S17b. Then, the coin cell is clamped by a staple of the Land-2001A (Wuhan, China) automatic battery tester (Fig. S17c) and the VSP multichannel potentiostatic-galvanostatic system (Fig. S17d). We add the photograph of the electrochemical setup and the measurement system in the supporting information. (Fig. S17)

Table S1. Performance comparison of the alloying and conversion mechanism potassium-ion battery anodes reported in literature and this work.

Material	Reversible discharge capacity	Rate	Cycle life
Sn_4P_3@C[1]	399 mA h g^{-1} at 50 mA g^{-1}	221.9 mA h g^{-1} at 1000 mA g^{-1}	80 % after 50 cycles
CoS@G[2]	434.5 mA h g^{-1} at 500 mA g^{-1}	232.3 mA h g^{-1} at 4000 mA g^{-1}	56.2 % after 100 cycles
VS_2[3]	400 mA h g^{-1} at 100 mA g^{-1}	100 mA h g^{-1} at 2000 mA g^{-1}	105 % after 100 cycles
BP-C[4]	400 mA h g^{-1} at 25 mA g^{-1}	300 mA h g^{-1} at 2000 mA g^{-1}	61 % after 50 cycles
MoS_2[5]	65 mA h g^{-1} at 20 mA g^{-1}	53.8 mA h g^{-1} at 160 mA g^{-1}	97.5 % after 200 cycles
MoS_2@rGO[6]	679 mA h g^{-1} at 20 mA g^{-1}	178 mA h g^{-1} at 500 mA g^{-1}	108 % after 100 cycles
SnS_2@rGO[7]	350 mA h g^{-1} at 25 mA g^{-1}	120 mA h g^{-1} at 2000 mA g^{-1}	78.9 % after 30 cycles
Sn-C[8]	150 mA h g^{-1} at 25 mA g^{-1}	Not Provided	75 % after 30 cycles
3D-HPCS[9]	310 mA h g^{-1} at 50 mA g^{-1}	150 mA h g^{-1} at 500 mA g^{-1}	70 % after 100 cycles
Bi/rGO[10]	290 mA h g^{-1} at 50 mA g^{-1}	235 mA h g^{-1} at 500 mA g^{-1}	41.1 % after 50 cycles

Material	Reversible discharge capacity	Rate	Cycle life
SnO_2-G-C[11]	270.1 mA h g^{-1} at 100 mA g^{-1}	114.81 mA h g^{-1} at 1000 mA g^{-1}	61 % after 100 cycles
ReS_2/N-CNTs[12]	253 mA h g^{-1} at 50 mA g^{-1}	Not Provided	72.3 % after 100 cycles
Sb_2S_3-SNG[13]	537 mA h g^{-1} at 20 mA g^{-1}	340 mA h g^{-1} at 1000 mA g^{-1}	89.4 % after 100 cycles
MoS_2@SnO_2@C[14]	597 mA h g^{-1} at 50 mA g^{-1}	86 mA h g^{-1} at 800 mA g^{-1}	52.3 % after 25 cycles
Sb-C[15]	650 mA h g^{-1} at 35 mA g^{-1}	420 mA h g^{-1} at 175 mA g^{-1}	98 % after 50 cycles
Sn_4P_3@C[16]	403.1 mA h g^{-1} at 50 mA g^{-1}	169 mA h g^{-1} at 2000 mA g^{-1}	80 % after 1000 cycles
CoP@NPPCS[17]	174 mA h g^{-1} at 50 mA g^{-1}	54 mA h g^{-1} at 2000 mA g^{-1}	without detectable capacity fading after 1000 cycles
U-Co_2P@rGO-14 (this work)	374 mA h g^{-1} at 20 mA g^{-1}	141 mA h g^{-1} at 2000 mA g^{-1}	64.7 % in the first 200 cycles; 83.6 % during 200 to 5 ,000 cycles

References

1 W. Zhang, J. Mao, A. Li, Z. Chen, Z. Guo, *J. Am. Chem. Soc.*, 2017, **139**, 3316.

2 H. Gao, T. Zhou, Y. Zheng, Q. Zhang, Y. Liu, J. Chen, H. Liu, Z. Guo, *Adv. Funct. Mater.*, 2017, **27**, 1702634.

3 J. Zhou, L. Wang, M. Yang, J. Wu, F. Chen, W. Huang, N. Han, H. Ye, F. Zhao, Y. Li, Y. Li, *Adv. Mater.*, 2017, **29**, 1702061.

4 I. Sultana, M. M. Rahman, T. Ramireddy, Y. Chen, A. M. Glushenkov, *J. Mater. Chem. A*, 2017, **5**, 23506.

5 X. Ren, Q. Zhao, W. D. McCulloch, Y. Wu, *Nano Res.*, 2017,**10**, 1313.

6 K. Xie, K. Yuan, X. Li, W. Lu, C. Shen, C. Liang, R. Vajtai, P. Ajayan, B. Wei, *Small*, 2017, **13**, 1701471.

7 V. Lakshmi, Y. Chen, A. A. Mikhaylov, A. G. Medvedev, I. Sultana, M. M. Rahman, O. Lev, P. V. Prikhodchenko, A. M. Glushenkov, *Chem. Commun.*, 2017, **53**, 8272.

8 I. Sultana, T. Ramireddy, M. M. Rahman, Y. Chen, A. M. Glushenkov, *Chem. Commun.*, 2016, **52**, 9279.

9 K. Huang, Z. Xing, L. Wang, X. Wu, W. Zhao, X. Qi, H. Wang, Z. Ju, *J. Mater. Chem. A*, 2018, **6**, 434.

10 Q. Zhang, J. Mao, W. Pang, T. Zheng, V. Sencadas, Y. Chen, Y. Liu, Z. Guo, *Adv. Energy Mater.*, 2018, **8**, 1703288.

11 Z. Huang, Z. Chen, S. Ding, C. Chen, M. Zhang, *Mater. Lett.*, 2018, **219**, 19.

12 M. Mao, C. Cui, M. Wu, M. Zhang, T. Gao, X. Fan, J. Chen, T. Wang, J. Ma, C. Wang,. *Nano Energy*, 2018, **45**, 346.

13 Y. Lu, J. Chen, *Sci. China: Chem.*, 2017, **60**, 1533.

14 Z. Chen, D. Yin, M. Zhang, *Small*, 2018, **14**, 1703818.

15 W. D.McCulloch, X. Ren, M. Yu, Z. Huang, Y. Wu, *ACS Appl. Mater. Interfaces*, 2015, **7**, 26158.

16 W. Zhang, W. Pang, V. Sencadas, Z. Guo, *Joule*, 2018, **2**, 1.

17 J. Bai, B. Xi, H. Mao, Y. Lin, X. Ma, J. Feng, S. Xiong, *Adv. Mater.*, 2018, **30**, 1802310.